Evidence for Nonlinear Processes in Fostering a North Pacific Jet Retraction

by

MELISSA BREEDEN[1] and JONATHAN E. MARTIN[2]

[1]Space Science and Engineering Center
[2]Department of Atmospheric and Oceanic Sciences
University of Wisconsin-Madison
1225 W. Dayton St.
Madison, WI 53706
608-262-9845
jemarti1@wisc.edu

Keywords: jet stream variability, vortex-vortex interactions, north Pacific atmospheric variability, midlatitude weather systems

ABSTRACT

A diagnostic method for calculating local geostrophic wind tendencies in a piecewise manner within the quasi-geostrophic framework is introduced. The method is applied to a case study of a North Pacific jet retraction that occurred in February 2006, and reveals that nonlinear interactions, which are dependent upon the phasing between potential vorticity anomalies and height anomalies, lead to a weakening of the jet. The synoptic context in which nonlinear advection weakens the jet is presented, revealing that a positively-tilted wave train situated north of the jet is conducive to retraction. This circumstance is consistent with conditions associated with barotropic energy extraction in which the growth of eddies occurs at the expense of the kinetic energy of the mean state. The relationship between this new method and existing methods of assessing geostrophic wind tendencies is explored and, though broad consistency is found, importance differences are identified and considered.

1. Introduction

The zonal extension or retraction of the tropopause-level jet stream is intimately linked to the position and strength of a host of extratropical disturbances including cyclones, blocks, and atmospheric rivers (Berggren et al. 1949; Rex 1950; Martius et al. 2007; Jaffe et al. 2011; Handlos and Martin 2016; Griffin and Martin 2017). In the north Pacific, the zonal pulsing of the jet exit region between 160°E – 160°W dominates 250-300 hPa zonal wind variability (Eichelberger and Hartmann 2007; Athanasiadis 2010; Jaffe et al. 2011; Griffin and Martin 2017). The retracted phase of this pulsing north Pacific jet, wherein the jet exit region is nearer its western limit, is associated with more frequent subtropical cyclogenesis in the central part of the basin and midlatitude blocking in the north (Otkin and Martin 2004; Breeden and Martin 2018). While periods of retraction and the attendant wavy (and often blocked) flow are well-known forecast challenges, and are associated with notable sensible weather impacts such as flooding and extreme cold (Hoskins and Sardeshmukh 1987; Otkin and Martin 2004; Jayawardena and Chen 2011), a complete understanding of the transition to such a retracted state is lacking in the current literature. Various physical mechanisms for blocking onset and blocking maintenance have been attributed to deformation, vortex-vortex interactions, diabatic heating and tropical convection, but consensus regarding which of these processes is the most important has not yet been achieved (Shutts 1983; Frederiksen 1983; Yamazaki and Itoh 2013; Pfahl et al. 2015; Henderson et al. 2016).

Shutts (1983) discussed how transient disturbances lead to the continued differential advection of low-PV into a midlatitude block, thereby reinforcing the block. Andrews and McIntyre (1976) first linked eddy momentum and temperature flux convergence, as represented by the Eliassen-Palm (E-P) flux convergence, to a weakening or strengthening of the zonal mean,

zonal wind. Hoskins et al. (1983), Plumb (1985) and Trenberth (1986) all presented formulations that expanded the two-dimensional E-P flux diagnostics to three dimensions, often referred to as the **E**-vector, and demonstrated how this diagnostic can be used to study changes in the geostrophic wind. The key insight is that differential **E**-vector convergence is linked to flux convergence of the quasi-geostrophic potentival vorticity (QGPV), the forcing for lagrangian changes in low-frequency QGPV, and thus influences the gradient of QGPV upon which the geostrophic wind is dependent. In this study, we extend QG piecewise tendency diagnosis (PTD, Nielsen-Gammon and Lefèvre 1996), traditionally used to investigate height tendencies associated with an amplifying synoptic wave, to investigate the various physical processes and their direct influence upon the Eulerian tendency of the geostrophic *wind*. In doing so we attain physical insights similar to those gained by the **E**-vector perspective but through an Eulerian perspective unconstrained by assumptions of a zonally symmetric basic state, which applies to either transient or stationary features. The way in which PTD can be utilized to combine information about eddy lifecycles with their direct impact on the zonal wind is also considered.

Breeden and Martin (2018) examined a long-lived jet retraction that began in mid-February 2006 and was associated with persistent Hawaiian precipitation and flooding. The synoptic overview of the case showed that anticyclonic (LC1) wave breaking events in the 315-330K isentropic layer facilitated retraction (Features A, B in Figure 1; their Figure 5). First, Feature A amplified in the central Pacific from 11-15 February (Figure 1a-c), and proceeded to overturn anticyclonically thereafter (Figure 1d). Feature B moved through the jet core in the 315-330K layer from 13-16 February, becoming superposed with A by 19 February (Fig 1e). To investigate the initial weakening of the jet, the lifecycle of A was diagnosed using the PTD methodology introduced by Nielsen-Gammon and Lefèvre (1996). PTD employs QGPV

inversion to identify various physical processes that influence the lifecycle of a growing synoptic disturbance using QG height tendencies. Application of PTD to Feature A revealed that large-scale deformation in the background state governed the amplification of the ridge, and in concert with baroclinic amplification and nonmodal growth, Feature A was able to grow rapidly in magnitude and size in the central Pacific.

In this paper, the PTD methodology is expanded to quantify the explicit contributions from various physical processes, all distinguishable by PTD, to jet retraction; the deceleration of the jet in its exit region. The expanded PTD methodology is outlined in Section 2 and its use is applied to the initial stage of the 2006 jet retraction in Section 3. Discussion and conclusions comparing this diagnostic to other studies related to jet stream variability are presented in Section 4.

2. Data and Methodology

This study employs European Centre for Medium-Range Weather Forecasting (ECMWF) ERA-interim gridded data, accessed at 1°x1° spatial resolution and six hourly temporal resolution, via the online archive (Dee et al., 2011). The ERA-Interim data set optimally combines observations (including those from polar orbiting and geostationary satellites) using a four-dimensional variational analysis (4D-Var) scheme, with model output, to create a Reanalysis dataset from 1979 to present. Geopotential was accessed on pressure surfaces from 50-1000 hPa at 50 hPa intervals and was used for QGPV inversion, as well as height and geostrophic wind tendencies. 300 hPa height anomalies were calculated with respect to the 11-15 February 2006 average subtracted at each available time. Height tendencies at each grid point were computed using a 12-hour, centered finite difference approximation,

$$\frac{\partial \phi}{\partial t} = \frac{\phi(t+1) - \phi(t-1)}{2\Delta t} \quad (1)$$

where $\Delta t = 6$ hours. We will call these the 'observed' height tendencies, which will be compared to those anticipated by the QG system.

The dynamic tropopause was considered in terms of Ertel (1942) potential vorticity on the 2 PVU surface (1 PVU = 10^{-6}K kg^{-1}m^{2}s^{-1}). Potential temperature (θ) on the 2 PVU surface is provided by ECMWF, and is determined by identifying the first observation of the 2 PVU value below 98 hPa, and then evaluating θ at that grid point (Berrisford et al., 2011). If the 2 PVU value is not located below 98 hPa, no value of θ is included in the data set. Potential temperature anomalies from the long term mean were computed with respect to the 1979-2016 average at each available time, and then were averaged to a daily mean.

2.1 Extended Piecewise Tendency Diagnosis

The traditional PTD methodology was explained and applied in detail in Nielsen-Gammon and Lefèvre (1996) and Breeden and Martin (2018). If one assumes that quasi-geostrophic potential vorticity (QGPV, given in Equation 2) is conserved following geostrophic motion, QG height tendencies are directly related to geostrophic QGPV advection (Equation 3).

$$q = f + \frac{1}{f_o}\nabla^2\phi + f_o\frac{\partial}{\partial p}\left(\frac{1}{\sigma}\frac{\partial\phi}{\partial p}\right) = f + \mathcal{L}(\phi) \qquad (2)$$

$$\frac{\partial\phi}{\partial t} = \mathcal{L}^{-1}\left(\frac{\partial q}{\partial t}\right) = \mathcal{L}^{-1}(-\boldsymbol{v}_g \cdot \nabla q) \qquad (3)$$

Inverting advection will yield the corresponding QG height tendencies. By defining a basic state (overbars) and perturbations around that basic state (primes), and splitting the atmosphere into an upper and lower layer (denoted by subscripts *u* and *l*, respectively), advection can be split into several components that represent distinct physical processes. Equation 4 below includes only the terms that contribute to upper-level height tendencies.

i *ii* *iii*

$$\frac{\partial \phi'_u}{\partial t} = \mathcal{L}^{-1}\left(-\overline{\boldsymbol{v}}_g \cdot \nabla q'_u\right) + \mathcal{L}^{-1}\left(-\boldsymbol{v}'_{gu} \cdot \nabla \overline{q}_u\right) + \mathcal{L}^{-1}\left(-\boldsymbol{v}'_{gl} \cdot \nabla \overline{q}_u\right) \quad (4)$$

$$+ \underbrace{\mathcal{L}^{-1}\left(-\boldsymbol{v}'_{gu} \cdot \nabla q'_u\right)}_{iv} + \underbrace{\mathcal{L}^{-1}\left(-\boldsymbol{v}'_{gl} \cdot \nabla q'_u\right)}_{v} + \underbrace{\mathcal{L}^{-1}\left(-\overline{\boldsymbol{v}}_g \cdot \nabla \overline{q}\right)}_{vi}$$

The terms in Equation (4) include effects of tropopause-level deformation (Term *i*), downstream development (Term *ii*), baroclinic amplification (Term *iii*), perturbation nonlinear vortex-vortex interactions (Terms *iv* - *v*) and basic state nonlinear interactions (Term *vi*). For the time mean basic state used in this analysis, Term *vi* is equal to zero, but for a mean and perturbation partition based upon spatial scale, can be non-zero. Tracking the height tendencies at the center of a growing wave provides a way to diagnose which processes contribute to intensification over the wave's lifecycle. If positive height tendencies from a given term overlap with a geopotential height maximum, for instance, that term promotes development, while negative height tendencies would indicate that term acts to weaken the height maximum. The sum of all terms indicates whether the anomaly strengthens or decays overall. For a more in-depth explanation of each term, the reader is referred to Nielsen-Gammon and Lefèvre (1996) or Breeden and Martin (2018).

i. Geostrophic Wind Tendency Equations

While understanding the lifecycle of features that facilitate retraction is illuminating, the amplification of a given ridge or trough alone does not directly correspond to a specific impact on the zonal wind. Rather, the movement of eddies, as represented by their associated height tendencies, leads to changes in geostrophic wind speed. Taking the local time derivative of the geostrophic wind and rearranging the partial derivatives yields a relationship between the local time tendency of the geostrophic wind and the horizontal gradient of local height tendencies:

$$\frac{\partial u_g}{\partial t} = -\frac{1}{f}\frac{\partial}{\partial y}\left(\left(\frac{\partial \phi}{\partial t}\right)\right) = -\frac{1}{f}\frac{\partial}{\partial y}\left(\mathcal{L}^{-1}\left(\frac{\partial q}{\partial t}\right)\right) \quad (5a)$$

$$\frac{\partial v_g}{\partial t} = \frac{1}{f}\frac{\partial}{\partial x}\left(\left(\frac{\partial \phi}{\partial t}\right)\right) = \frac{1}{f}\frac{\partial}{\partial x}\left(\mathcal{L}^{-1}\left(\frac{\partial q}{\partial t}\right)\right) \quad (5b)$$

Equation (5) reveals that if, in a certain location, the meridional gradient of height tendencies is positive, then the right-hand-side of Equation (5a) is negative, and the zonal geostrophic wind will weaken at that location (Figure 2). If, as in the schematic and the 2006 retraction, a ridge is located poleward of the mean jet axis, the ridge's movement will weaken the mean westerly flow. A similar tendency to weaken the zonal wind occurs on the northern branch of a trough, so a trough located *south* of the jet axis would similarly decelerate the jet. The aforementioned impact of troughs and ridges on the flow is far from a novel revelation, but when waves are periodic the influence on the geostrophic wind is often short-lived. By definition jet retractions require that the zonal wind is weakened substantially (at least 10 m s^{-1} below climatology in the vicinity of the jet exit region, (Jaffe et al., 2011)) and for at least five days. As such, an impact beyond the transient, periodic movement of waves along the jet must be achieved by the eddies to explain the associated long-lived transition of the jet. Determining which of the terms isolated in PTD accounts for this transition is the primary focus of this analysis.

Assuming QGPV is conserved following the geostrophic flow, geostrophic QGPV advection can be substituted for $\frac{\partial q}{\partial t}$ in Equation (5a), and the same partitioning of advection as done in traditional PTD can be applied:

$$\frac{\partial u_g}{\partial t} = -\frac{1}{f}\frac{\partial}{\partial y}\left\{\begin{array}{l}\mathcal{L}^{-1}\left(-\overline{v}_g \cdot \nabla q'_u\right) + \mathcal{L}^{-1}\left(-\boldsymbol{v}'_{gu} \cdot \nabla \overline{q}_u\right) + \mathcal{L}^{-1}\left(-\boldsymbol{v}'_{gl} \cdot \nabla \overline{q}_u\right) \\ + \mathcal{L}^{-1}\left(-\boldsymbol{v}'_{gu} \cdot \nabla q'_u\right) + \mathcal{L}^{-1}\left(-\boldsymbol{v}'_{gl} \cdot \nabla q'_u\right) + \mathcal{L}^{-1}\left(-\overline{\boldsymbol{v}}_g \cdot \nabla \overline{q}\right)\end{array}\right\} \quad (6)$$

Equation (6) demonstrates that the local weakening and strengthening of the geostrophic wind can be diagnosed in a piecewise manner, similar to that by which height tendencies were diagnosed in traditional PTD. Here the zonal wind component alone is emphasized, as retractions are defined based upon zonal wind variability, which dominates jet variability in the north Pacific (Athanasiadis et al. 2009; Griffin and Martin 2017). One may track the changes to the zonal wind following a certain anomaly, such as Feature A, in a manner similar to that in which the maximum height anomaly associated with Feature A was tracked and diagnosed. Alternatively, it is possible to choose one location – for example, the jet exit region – and explore the processes accelerating the zonal wind in that region through time. Consistent with the Eulerian definition of jet retractions presented by Jaffe et al. (2011), the latter approach is used to understand how retraction was initiated in February 2006. Recall that the jet exit region in the central Pacific coincides with the location of greatest amplitude in the EOF1 pattern of the 300-250 hPa zonal wind (Figure 4 from Jaffe et al. 2011). The next section investigates the cumulative influence of Features A and B on retraction from 11-15 February, using the same PTD results presented in Breeden and Martin (2018).

3. Results from Applying Piecewise Zonal Wind Tendency Diagnosis

Figure 3 shows the integrated zonal geostrophic wind change from 11-15 February, attained by summing the zonal wind change at every grid point, over each 6-hourly time step in the five-day period. Over this five-day period the zonal wind weakened substantially along the southern portion of the jet core as well as in its exit region near 160°W. Understanding what features and, through Equation (6), what processes contributed to the retraction/deceleration of the zonal jet is the focus of the ensuing analysis. Retractions are focused on weakened zonal flow specifically within the climatological jet exit region in the central north Pacific, often

associated with a split jet and a dipole-type block (Jaffe et al. 2011). Figure 4 shows the time series of the deceleration calculated in a variety of ways, averaged over an area encompassing the jet exit region (green box in Figure 3). To ensure the deceleration captured by the anomalous, upper-level height field accurately represents the change in the unpartitioned height field, the local deceleration was calculated using the height anomaly field attained from inverting upper-level (50-500 hPa) perturbation QGPV, q'_u, Equation (7), subsequently calculating ϕ'_u tendencies via Equation (1).

$$\phi'_u = \mathcal{L}^{-1}(q'_u) \qquad (7)$$

The close match between the two time series in Figure 4a confirms that the basic state definition does not inhibit application of PTD via Equation (6) to diagnose the processes involved in retraction. Both fields indicate that the zonal wind in the jet exit region weakened from 11-12 February, temporarily strengthened on 13 February, and then weakened from 14-15 February.

To quantify the net change in the zonal wind associated with the upper-level QGPV structure, the area under the blue line in Figure 4b was integrated, corresponding to an overall wind speed change of -32 m s^{-1} from 0000 UTC 11- 1800 UTC 15 February. The cumulative deceleration attained using the QG height tendencies output by PTD using (6) accounts for -25m s^{-1}, 78% of the retraction associated with upper-level QGPV (red line Figure 4b), confirming that the PTD method can explain the majority of the observed retraction of the jet exit region in this case.

3.1 Piecewise Zonal Wind Tendency Results

The terms that drove the amplification of Feature A (Terms *i* and *iii*; Breeden and Martin 2018) are not necessarily the same terms that contributed most to the jet retraction. Figure 5 shows the time series of the deceleration arising from the five terms in Equation (6), revealing

that the highest-magnitude term is Term *i,* the propagation/deformation term, $\left(-\overline{v}_g \cdot \nabla q'_u\right)$, which oscillates in concert with the total deceleration. This term includes the advection of ridges and troughs by the time mean geostrophic wind, so a large contribution from this term is not surprising. Term *ii,* the downstream development term, $\left(-\boldsymbol{v}'_{gu} \cdot \nabla \overline{q}_u\right)$, represents the advection of the background QGPV gradient by the circulation associated with QGPV anomalies and varies inversely with the advection/deformation term and the total deceleration. As an example, consider how the northerly flow on the western side of a trough will lead to positive background QGPV advection and height falls, reflecting the trough's tendency to propagate upstream relative to the background wind. This upstream propagation is opposed by the background wind's tendency to advect the trough downstream, producing height *rises* west of the trough. As a result, the advection/deformation and downstream development terms are anticorrelated.

Term *iii,* the baroclinic development term, $\left(-\boldsymbol{v}'_{gl} \cdot \nabla \overline{q}_u\right)$, first negated retraction on 11 February and then promoted it from 12-13 February. Thereafter this process made barely any direct contribution to the zonal geostrophic wind tendency. Interestingly, Term *iv*, upper-level, nonlinear vortex-vortex interactions, $\left(-\boldsymbol{v}'_{gu} \cdot \nabla q'_u\right)$, which had a markedly weaker influence on the amplification of Feature A than the previous terms, systematically contributed to retraction throughout the five days. The contribution to retraction from Term *v,* low-level nonlinear interactions, oscillated closely around zero.

It was previously noted that the instantaneous change in zonal wind is heavily influenced by the transient movement of eddies into and out of the region where retractions are identified. The deformation and downstream development terms clearly demonstrate this oscillatory behavior. To eliminate the transient effect of waves propagating eastward, the changes in zonal wind from each term in Equation (6) were integrated individually over the five-day period, by

integrating the area under each curve in Figure 5. The results shown in Table 1 reveal that the integrated effects of all terms *except* upper-level nonlinear vortex interactions are near zero. Of course, the integrated contributions for the deformation, downstream development and baroclinic development terms *must* be near zero, since the integration was performed over the same period in which the anomalies were defined. The only terms that are not constrained to be zero in the integration are the nonlinear, vortex-vortex interaction terms, Terms *iv* and *v*. Interestingly, in this case it is found that just one of these terms, the upper-level nonlinear interactions, contributed to nearly all of the -25 ms^{-1} deceleration. The context in which this was achieved follows in the next sub-section.

Figure 6 shows the spatial maps of the integrated terms from 11-15 February, confirming that the deformation, downstream development and baroclinic development components are near zero everywhere in the domain as required by the basic state definition. The two nonlinear terms exhibit strong, often opposing dipoles of acceleration and deceleration that straddle the jet meridionally. However, the upper-level term ultimately dominates the influence of the lower-level term (Figure 6e-f), as Figure 6e bears a notable resemblance to the total in Figure 6a. Local deceleration associated with upper-level nonlinear advection was located within the jet exit region and southern portion of the jet core, accounting for the retraction diagnosed by the QG system. This result is consistent with the perspective of Hoskins et al. (1983) and Shutts (1983), who both emphasized nonlinear potential vorticity flux convergence as the forcing to weaken the *Lagrangian* tendency of the QGPV. If the QGPV tendencies are non-uniform, the QGPV gradient will also change, corresponding to changes in the zonal wind.

i. Investigation of Upper-level, Vortex-Vortex Interactions

To contextualize the conditions during which upper-level, nonlinear interactions produced retraction, Figure 7a shows the 12 February mean forcing for the upper-level vortex interaction term, with the associated positive height tendency response shown in Figure 7b. The fill in Figure 7a shows the q'_u anomalies that are advected by $\boldsymbol{v}'_{gu}$ shown by the arrows. Recall that $\boldsymbol{v}'_{gu}$ is computed from ϕ'_u, which in turn is related to the same q'_u field that is being advected. Due to the slight offset between ϕ'_u and q'_u (resulting from the non-local influence of each QGPV anomaly in the domain) the geostrophic circulation $\boldsymbol{v}'_{gu}$ is not perfectly parallel to isopleths of q'_u and thus advection is possible.

Regions of negative QGPV advection produce positive height tendencies (Equation (3)), which are, in turn, associated with deceleration on their southern edge (Figure 2; Equation (5a)). Negative QGPV advection is particularly notable on the eastern portion of Feature A, at this time located at 45°N, 175°E, with strong northerly winds advecting q'_u to the south. In fact, both Features A and B are associated with strong, negative q'_u anomalies that were greatest in magnitude near 45°N, and northerly flow on each anomaly's eastern side advected low q'_u southward. Simultaneously, southerly flow on the western side of A and the eastern flank of the trough upstream advected subtropical negative q'_u northward, coinciding with negative q'_u advection and also producing height rises. As a result of the coordinated negative q'_u advection associated with A, B and the trough in between, a continuous region of height rises extends from 110°E-160°W (Figure 7b), and to their south, a negative zonal geostrophic wind tendency was produced (Figure 7c, blue contours). The location of the negative zonal wind tendency with respect to the zonal jet on 12 February confirms that both the exit region and southern edge of the jet core were induced to weaken by this term.

All three height anomalies associated with negative q'_u advection were positively tilted on 12 February, the day marking the strongest forcing for deceleration during the five day period. The cumulative influence of this process on height rises and deceleration is confirmed from inspection of the five-day mean height tendencies and deceleration in Figure 8. The negative zonal geostrophic wind tendency located along the southern portion of the jet in Figure 8 indicates that nonlinear, negative QGPV advection, specifically that achieved by $\boldsymbol{v}'_{gu}$, systematically occurred throughout the jet axis during this five day period.

4 Discussion and Conclusions

In this paper a novel perspective for understanding geostrophic wind speed changes through extension of the PTD diagnostics introduced by Nielsen-Gammon and Lefèvre (1996) was presented. It was shown that the simple relationship between horizontal gradients in height tendencies and changes in the geostrophic wind holds for instantaneous or time-averaged changes in the geostrophic wind. This relationship can be combined with piecewise tendency analysis to split the total deceleration field into contributions from various, distinct processes, and can be used to eliminate the transient effect of wave propagation without requiring time or zonal averaging. The extended approach was applied to investigate the onset of a long-lived north Pacific jet retraction in mid-February 2006. Specifically, the influence of a wave train containing positively-tilted, potent anticyclonic anomalies A and B north of the jet axis on the local deceleration that initiated retraction was quantified.

The instantaneous changes in the zonal wind were heavily influenced by mean-flow advection of anomalies, while the cumulative 11-15 February retraction was dominated by nonlinear vortex-vortex interactions – specifically, differential negative q'_u advection by the winds associated with the q'_u field itself. The net flux of low QGPV from the tropics/subtropics

northward is commonly the way in which nonlinear advection is viewed as a mechanism that prevented the zonal wind from strengthening in blocking regions (Hoskins et al. 1983, Crum and Stevens 1988). In this case, negative QGPV anomalies associated with Features A and B were differentially advected *southward* (Figure 7), weakening the zonal wind along the southern edge of the jet core and exit region. Anticyclonic anomalies that reach the poleward side of the jet, as observed in this case and in many retractions (see Figure 9 from Jaffe et al. 2011), may have a unique ability to influence the zonal wind given the relative position of their associated nonlinear advection fields to the jet.

Some advantages to the expanded PTD approach to evaluating geostrophic wind tendencies are that it can be applied to instantaneous, time mean, or spatially filtered data, as the only assumption made is QGPV conservation. Acceleration of both the zonal and meridional components of the geostrophic wind can be diagnosed in this manner, for stationary or transient features. The expanded PTD method also provides detailed information about the lifecycle of eddies with their influence on the geostrophic wind within the same diagnostic framework. Finally, merging QGPV inversion with a zonal wind diagnostic allows for separate quantification of the influence of both lower- and upper-level QGPV structures on the tropopause-level jet. While only the upper-level, nonlinear term contributed to retraction in this case, there is no theoretical constraint suggesting that this should be generally true. Admittedly, one limitation to the method is the extent to which QGPV conservation is accurate, a constraint shared by many diagnostics such as those introduced by Hoskins et al. (1983), Plumb (1985) and Trenberth (1986).

Given that the basic state was defined as a five-day time mean in this study, the contribution to zonal wind tendencies from terms that reference only one anomaly field *must* add

up to zero when integrating over the five-day period. However, the same analysis was performed using a large-scale basic state definition (not shown), and yet the nonlinear terms still dominated the geostrophic zonal wind tendency. Thus the physical insights resulting from the present analysis, which are consistent with previous studies regarding blocking and nonlinear processes, appear to exhibit little dependence on the basic state definition.

4.1 Comparison with a traditional zonal wind diagnostic

The dominance of nonlinear vortex-vortex interactions in retracting the jet is consistent with discussion of the role of nonlinear interactions in changing the low-frequency QGPV as presented by Hoskins et al. (1983). They showed that the QG eddy vorticity flux divergence is proportional to the Lagrangian tendency of the low-frequency QGPV in the absence of sources and sinks:

$$\left(\partial_t + \overline{\boldsymbol{v_g}} \cdot \nabla\right)\overline{q} = -\nabla \cdot \overline{\boldsymbol{v_g}' q'} \qquad (8)$$

Where the right-hand-side of Equation (8) is negative, the Lagrangian tendency of QGPV is negative. Assuming the flux convergence (and thus QGPV tendency) are spatially heterogeneous, changes in the QGPV *gradient* and by extension the geostrophic wind, must arise. To investigate the relationship between the Eulerian changes in wind speed as diagnosed using Equation (6), versus the Lagrangian change in the QGPV via Equation (8), the eddy vorticity flux convergence was calculated, averaged from 11-15 February and using only the $\boldsymbol{v_{gu}}'$ wind field to be consistent with Term *iv*. Next the meridional gradient of that flux convergence, which implies a change in the meridional gradient of the QGPV (and thus to changes in the zonal geostrophic wind), was calculated, with results shown in Figure 9. Negative values of the gradient of the nonlinear eddy vorticity flux lead to a weakening of the low-frequency QGPV gradient moving with the geostrophic flow. Regions where QGPV gradient weakens, and thus

where the geostrophic wind would weaken, are observed within the jet core from about 130-170°E, 30-35°N, and in the entrance region at 100-125°E, 35-40°N (Figure 9). A negative zonal wind tendency is observed in the exit region at 40-45°N, 170°E as well, but the tendencies are weaker in magnitude than those observed in the jet core. In contrast the forcing from Term *iv* implies an equally strong tendency to weaken the zonal wind in both the jet core and exit region (Figure 8). There are indeed regions where the Lagrangian and Eulerian zonal wind tendencies differ, including the region from 40-45°N, 130-160°E where the two diagnostics anticipate opposite tendencies. To the north of the negative geostrophic zonal wind tendencies observed in both diagnostics are regions of positive zonal wind tendencies, suggesting that from 11-15 February the mean QGPV gradient and jet core were forced to shift northward by the eddy fluxes.

The change in the jet structure associated with the beginning of retraction is presented Figure 10, which shows the daily mean QGPV and zonal wind on 11 February (Figure 10a) and 15 February (Figure 10b). It is evident that the QGPV gradient and jet core strengthened to the north and weakened to the south during this period, just as the two diagnostics compared in Figure 8 and Figure 9 would suggest. In particular, near-zero PV air was located near 30°N on 11 February, and shifted northward to 40°N by 15 February, revealing that a northward shift of the jet core accompanied the retraction of the exit region. Arguably the Eulerian perspective better explains the evolution of the jet in this manner than the more spatially-detailed Lagrangian perspective.

4.2 Conclusions

An important characteristic of the 2006 retraction was related to the propagation of anticyclonic anomalies on the poleward side of the jet and their impact upon the zonal wind. The

cumulative influence of anticyclonic anomalies A and B, and the trough located in between, on the zonal wind manifested itself through nonlinear interactions, which dominated the QG zonal wind tendencies from 11-15 February. Nonlinear advection was strongest on 12 February, coinciding with the time during which the wave train was most positively-tilted. Mak and Cai (1987) demonstrated that a positively tilted eddy in a region of cyclonic shear, a form of deformation, was conducive to the barotropic growth of the eddy at the expense of the kinetic energy of the environment. Here the retraction, and simultaneous amplification of Feature A (largely due to deformation), indicates that a barotropic energy exchange in which kinetic energy from the environment was transferred to kinetic energy of anomalies, indeed occurred. In fact, the winds associated with the upper-level QGPV anomalies are what rearrange the upper-level QGPV anomalies, indicating that the upper-level vortex-vortex term is by nature barotropic. Ongoing research suggests that a configuration involving positively-tilted height anomalies on the cyclonic shear side of the jet is often observed during jet retractions, for the reasons shown in Section 3.1, Figure 7.

The dominant influence of nonlinear, vortex-vortex interactions in facilitating jet retraction, attained through a novel expansion of QG piecewise tendency diagnosis to evaluation of geostrophic wind tendencies, is consistent with Shutts's perspective on blocking, which emphasized the role of eddy vorticity flux convergence as an important force that prevents the westerlies from reforming within the blocking region. More recently, Yamazaki and Itoh (2013) proposed an alternative way by which vortex-vortex interactions can impact the storm track and blocking through a 'selective absorption mechanism'. They considered the dominant interaction as one where eddies of different sizes impose different net accelerations on the eddies surrounding them. In such a manner they suggested that a blocking anticyclone preferentially

'attracts' smaller-scale anticyclones, maintaining the block. One key difference between the analysis presented in this study and previous diagnoses of blocking (implied as a negative zonal wind tendency) is the *zonally-elongated* band of height tendencies highlighted in this study, versus the isotropic region of flux convergence often associated with blocks in previous studies. This study has revealed the impact of a wave train with the right tilt and position relative to the jet, with the eddies all acting together to produce a large-scale effect on the circulation. There are, it appears, a variety of ways in which vortex-vortex interactions can alter the circulation. Future work will focus on generalizing these results to retractions in general and expanding the methodology to additional geographic regions. An attempt to forecast such jet stream transitions by viewing the nonlinear PTD terms in real time will also be an avenue of future research.

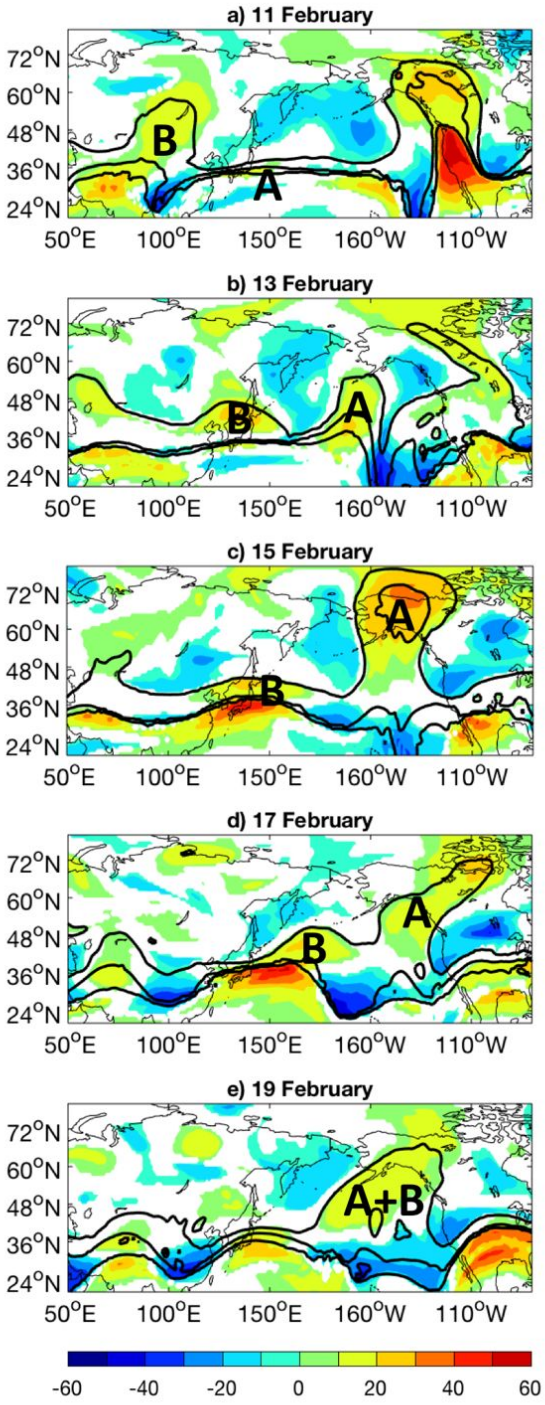

Figure 1: The fill shows the potential temperature anomalies on the 2PVU surface on a) 11 b) 13, c) 15 February, d) 17 February and e) 19 February 2006. Jet retraction criteria were met by 15-16 February (Jaffe et al., 2011). The potential temperature anomalies were calculated with respect to the 1979-2015 climatology for each day. The contours show the total 315, 330 and 345 K potential temperature surfaces on the 2 PVU surface at each time. Anticyclonic anomalies A and B are labeled.

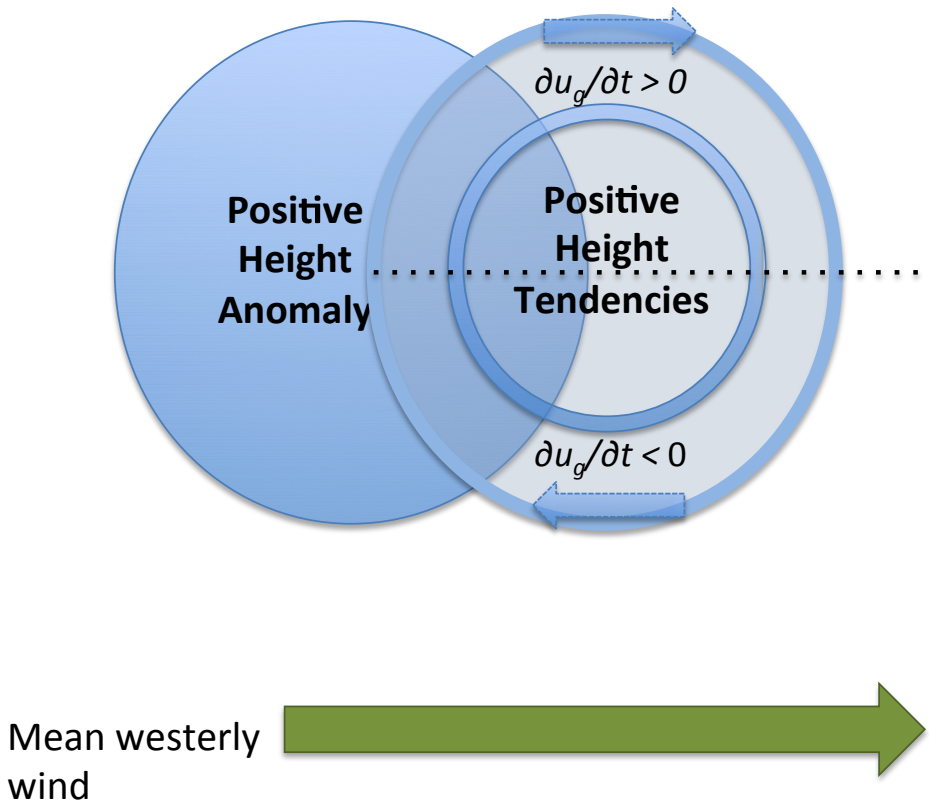

Figure 2: Schematic demonstrating the distribution of the local change in the geostrophic zonal wind around a positive height anomaly (see Equation 5a). Where height tendencies increase with latitude, the zonal wind will weaken, and where height tendencies decrease with latitude, the zonal wind will strengthen (blue arrows). Adding the blue arrows to a mean westerly wind on the ridge's southern edge indicates the effect of a ridge north of the jet, and its ability to weaken the zonal jet.

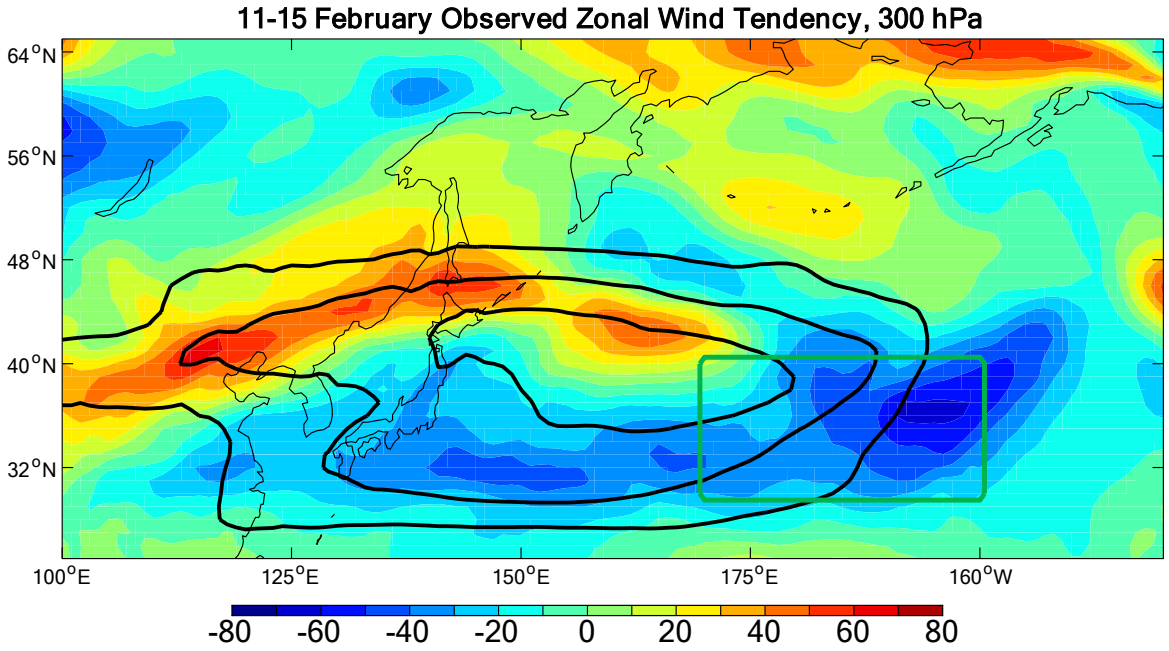

Figure 3: The color shading shows the 11-15 February change in zonal wind in m s^{-1}. The contours show the 11-15 February mean geostrophic zonal wind, contoured starting at 30 m s^{-1} every 10 m s^{-1}. The green box indicates the region over which the retraction is diagnosed.

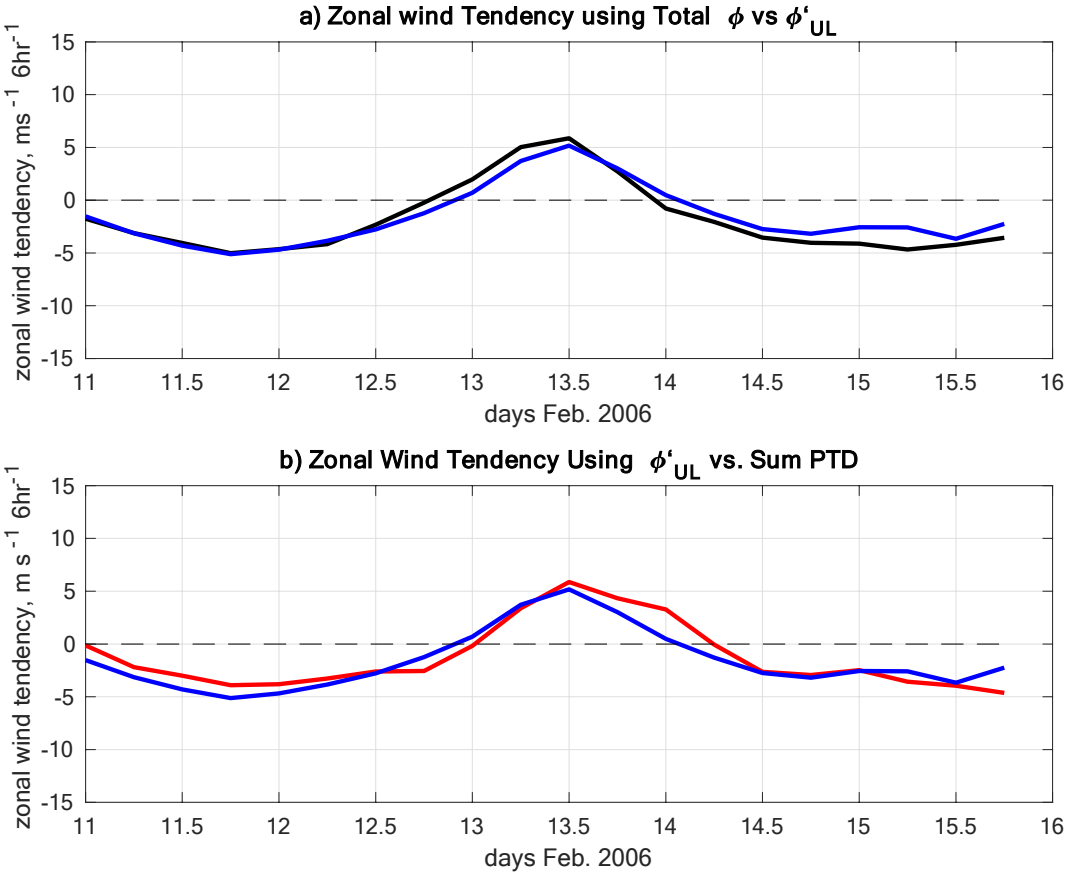

Figure 4: Time series tracking zonal wind change (units m s^{-1} (6 hr)$^{-1}$ averaged from 170-200°W, 30-40°N, from 11-15 February, using six-hourly data. a) shows zonal wind tendency using the total height field (black line) and the inverted height anomaly field associated with 50-500 hPa perturbation QGPV (blue line). b) The blue line is as in a), and the red line shows the zonal wind tendency explained using the height tendencies from PTD (Equation 6). The close correspondence between the time series provides confidence in the ability of the PTD methodology to explain the majority of the observed jet retraction.

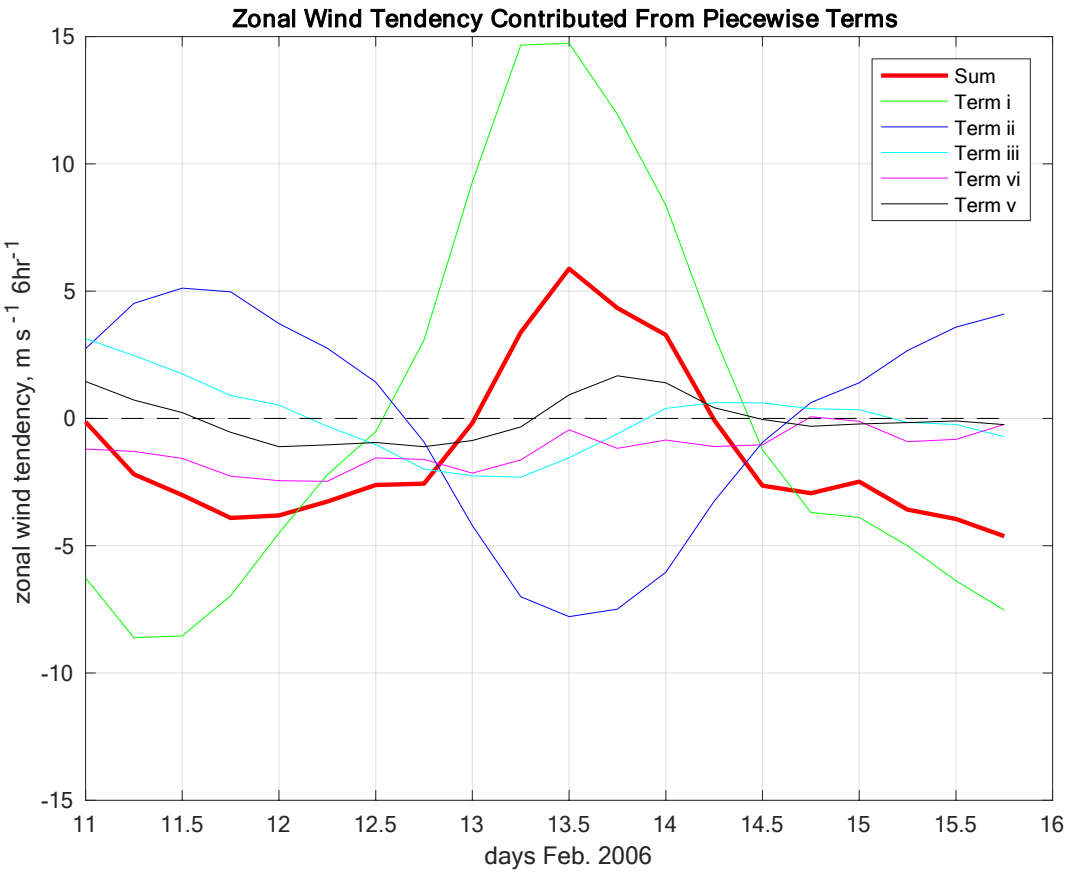

Figure 5: Time series of the individual PTD components' contribution to the zonal wind tendency using Equation 6, from 0000 UTC 11 1800 UTC 15 February. The red line is the sum of all terms, the green line is Term *i*, dark blue line Term *ii*, light blue line Term *iii*, pink line Term *iv*, and black line Term *v*, from Equation 6.

Height Field	**Integrated Zonal Wind Tendency (m s^{-1})**
q'_u - Derived Height Anomaly, ϕ'_u	-31.8388
Total PTD	**-25.1002**
Term *i*: Deformation/Superposition	-0.0079
Term *ii*: Downstream Development	-0.0186
Term *iii*: Baroclinic Development	-0.0100
Term *iv*: Vortex-vortex UL	-24.8444
Term *v*: Vortex-vortex LL	-0.2193

Table 1: Integrated tendency of the zonal wind from 0000 UTC 11 February – 1800 UTC 15 February 2006 using various height tendency fields.

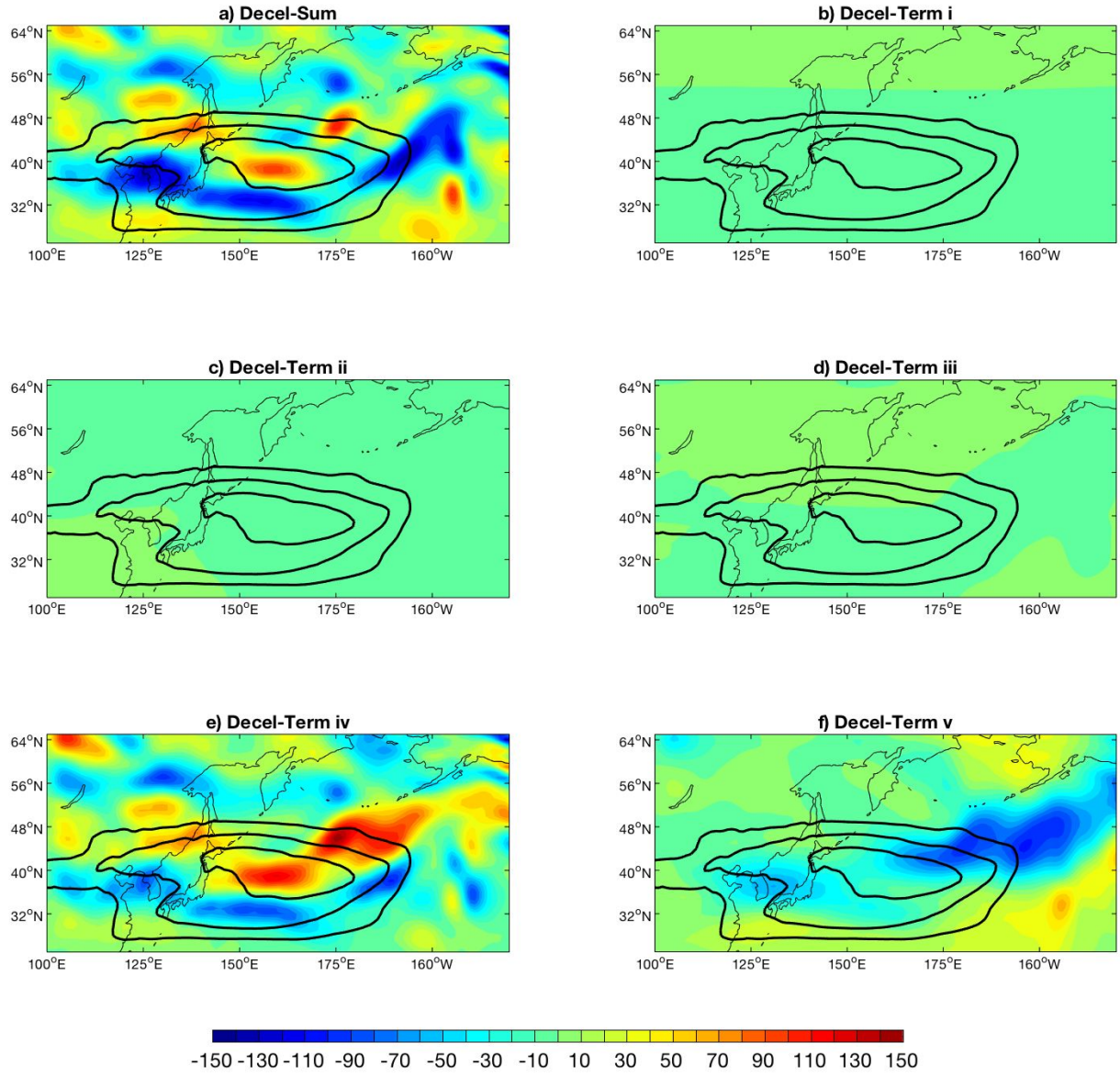

Figure 6: The color shading shows the 300 hPa integrated zonal wind tendency from 0000 UTC 11 February – 1800 UTC 15 February 2006 from terms in Equation (6) in m s^{-1}. a) shows the sum of Terms *i*-*v*, b) Term *i* (advection by mean flow, deformation, superposition), c) Term *ii* (downstream development), d) Term *iii* (baroclinic development), e) Term *vi* (upper-level vortex-vortex interactions), and f) Term *v* (low-level vortex-vortex interactions). The contours in each plot are the same and show the 11-15 February mean geostrophic wind, contoured starting at 30 m s^{-1} at intervals of 10 m s^{-1}.

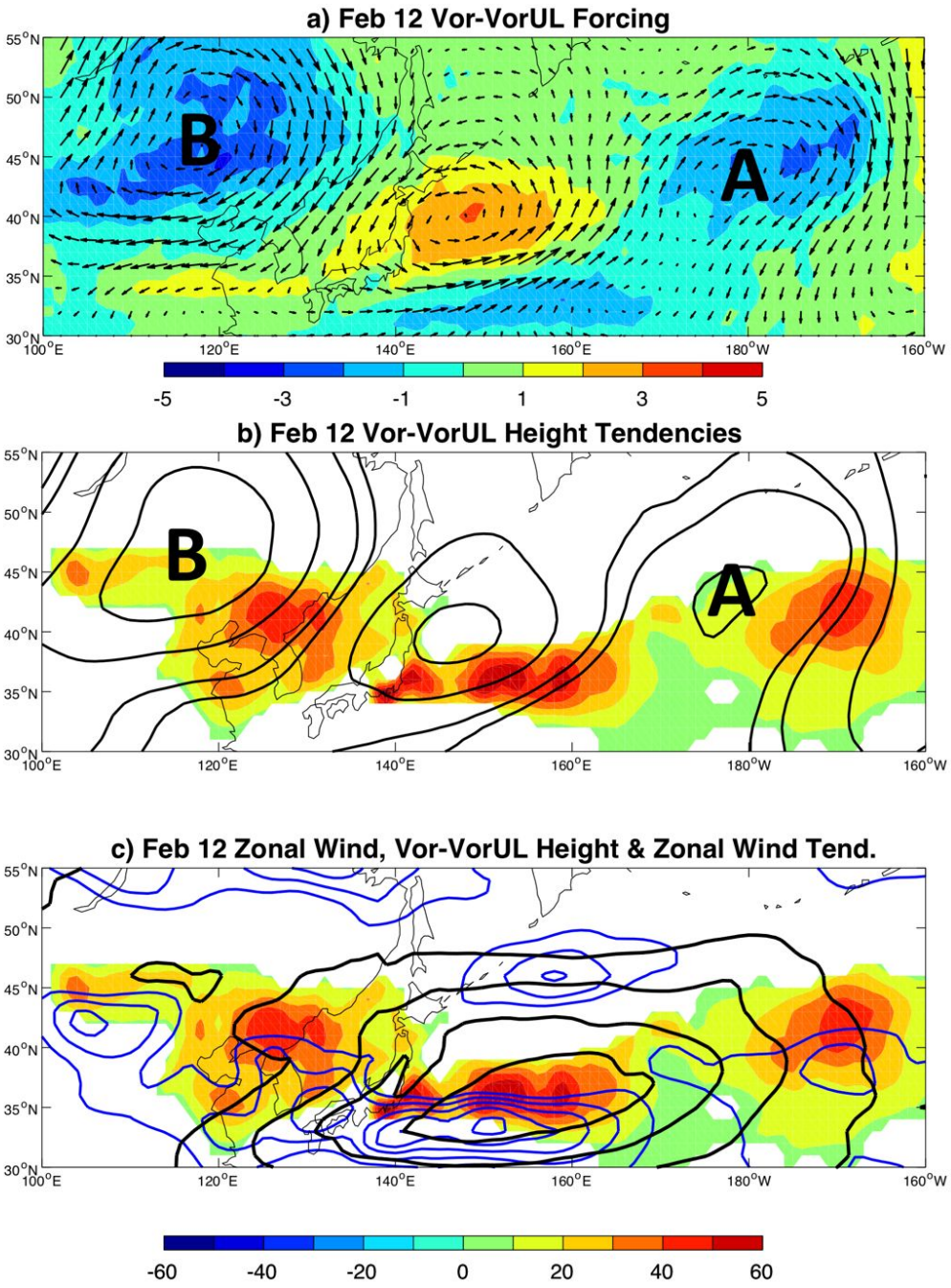

Figure 7: a) The color shading shows the 12 February average q'_u field in units of 10^{-4} s^{-1}. The black arrows show the 12 February average $\boldsymbol{v}'_{gu}$ field, which advects q'_u to produce height tendencies associated with the upper-level, nonlinear vortex interaction term. b) The color shading shows the 12 February averaged height tendencies associated with this term, whose forcing is shown in (a). Height tendencies are in units m $(6hr)^{-1}$, with positive values above 10 m $(6hr)^{-1}$ shown. The black contours show the 12 February average ϕ'_u field, contoured starting at +/- 20 m every 100 m. c) The color shading is the same as in (b), and the blue contours indicate the associated zonal wind tendency, contoured every 1 m s^{-1} beginning at -1 m s^{-1}. The black contours show the 12 February mean zonal wind, contoured every 10 m s^{-1} beginning at 30 m s^{-1}.

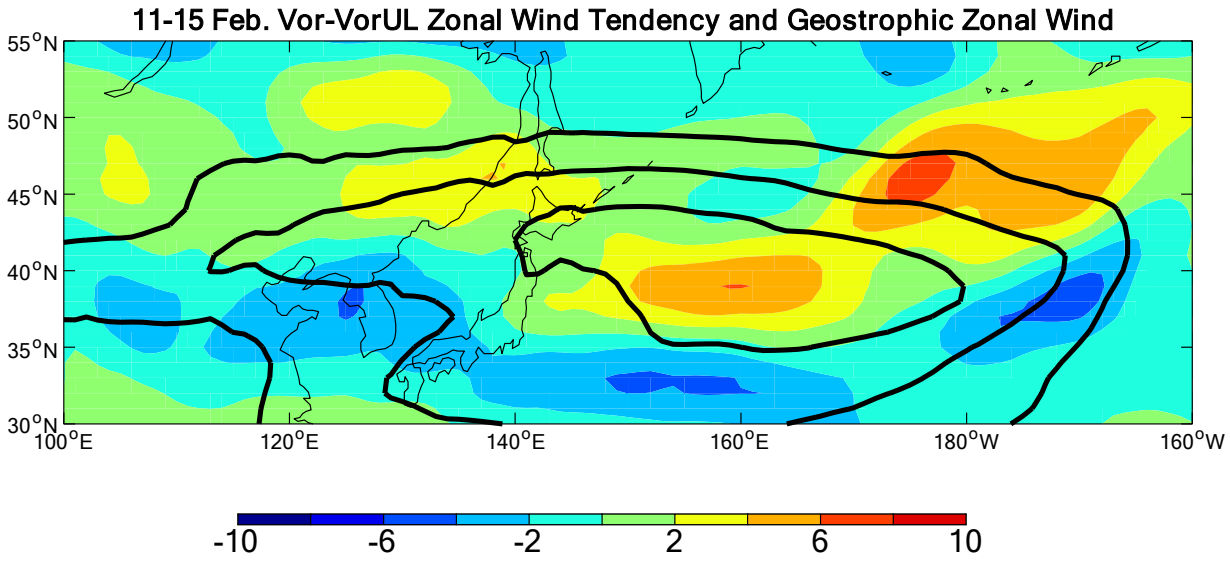

Figure 8: The color shading shows the 11-15 February average zonal wind tendencies associated with Term *iv*, upper-level nonlinear advection. The black contours show the 11-15 February zonal wind isotachs starting at 30 m s^{-1} every 10 m s^{-1}. The zonal wind tendency has units of m $s^{-1}(6hr)^{-1}$.

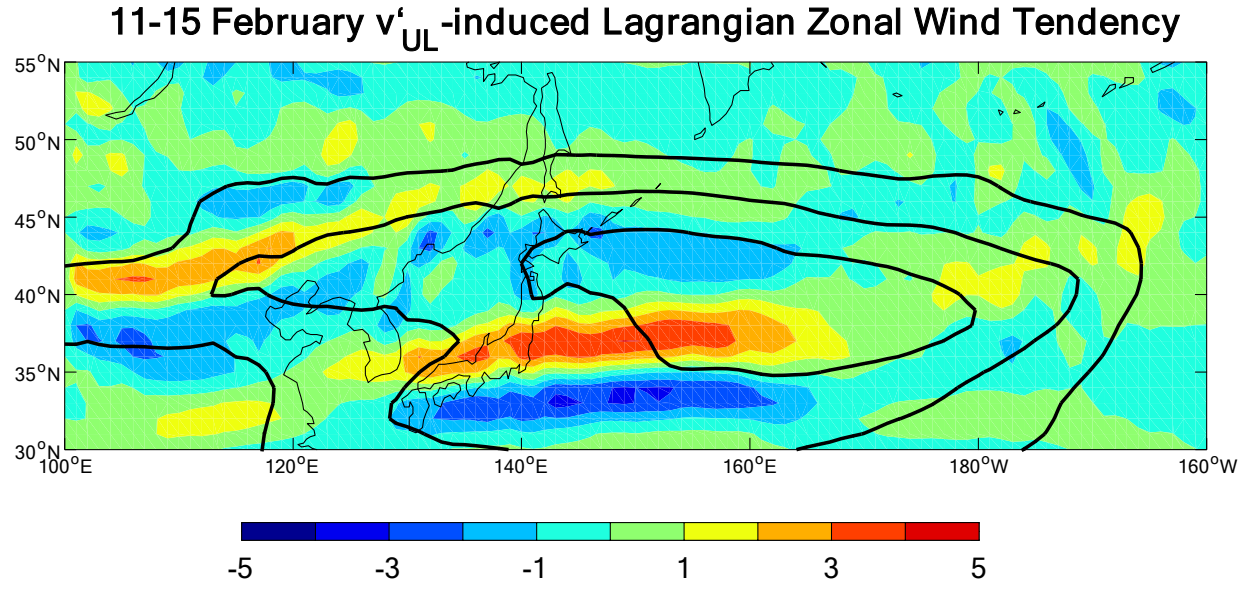

Figure 9: The color shading shows the 11-15 February mean meridional gradient of the eddy vorticity flux convergence (Equation (8)), which is proportional to the tendency of the upper-level QGPV gradient and zonal geostrophic wind. The geostrophic wind used was $\boldsymbol{v}'_{gu}$ for a direct comparison with Figure 8. Units are 10^{-14} m^{-1} s^{-2}. The contours are the 11-15 February mean geostrophic wind, contoured starting at 30 m s^{-1} every 10 m s^{-1}.

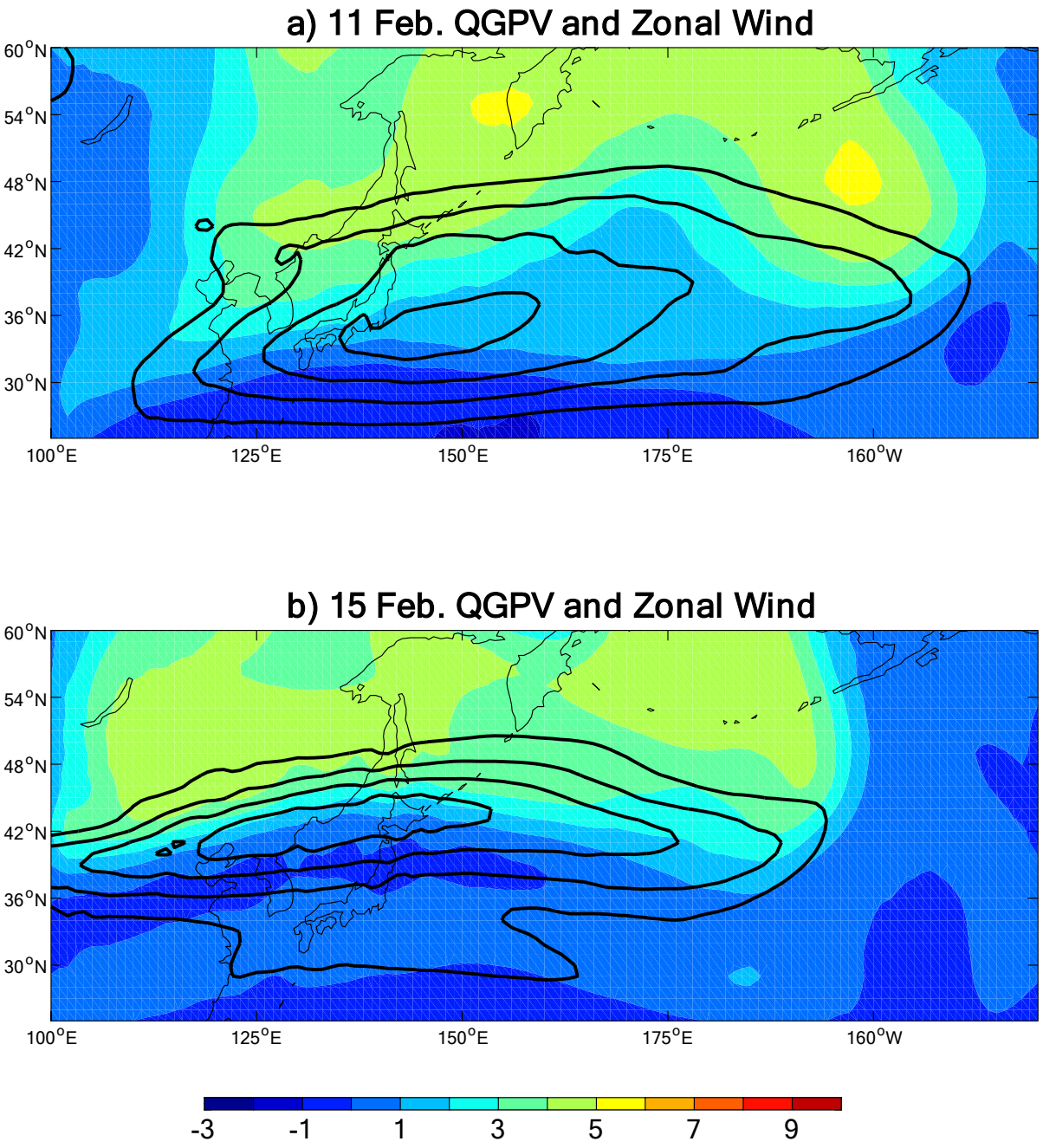

Figure 9: The color shading shows the daily mean QGPV and in contours is the zonal geostrophic wind on a) 11 February and b) 15 February 2006. Units of QGPV are 10^{-4} s^{-1}. Zonal wind contours begin at 30 m s^{-1} and increase at intervals of 10 m s^{-1}.

References

1. Andrews, D.G. and M.E. McIntyre, 1976: Planetary Waves in Horizontal and Vertical Shear: The Generalized Eliassen-Palm Relation and the Mean Zonal Acceleration. *J. Atmos. Sci.,* **33**, 2031–2048, https://doi.org/10.1175/1520-0469(1976)033<2031:PWIHAV>2.0.CO;2.

2. Athanasiadis P. J., J. M. Wallace, and J. J. Wettstein, 2010: Patterns of wintertime jet stream variability and their relation to the storm tracks. *J. Atmos. Sci.,* **67,** 1361-1381, doi:10.1175/2009JAS3270.1.

3. Berggren, R., B. Bolin & C.-G. Rossby (1949) An Aerological Study of Zonal Motion, its Perturbations and Break-down, Tellus, 1:2, 14-37.

4. Berrisford, P., D. P. Dee, P. Poli, R. Brugge, K. Fielding, M. Fuentes, P.W. Kållberg, S. Kobayashi, S. Uppala, and A. Simmons, 2011: The ERA-Interim archive Version 2.0. ERA Report Series 1, http://www.ecmwf.int/en/elibrary/8174-era-interim-archive-version-20.

5. Breeden, M. & J. E. Martin, 2018: Analyzing the onset of an extreme North Pacific Jet Retraction using Piecewise Tendency Diagnosis, *Quart. J. Roy. Meteor. Soc.*, 144-715, 1895-1913. doi: 10.1002/qj.3388.

6. Crum, F.X. and D.F. Stevens, 1988: A Case Study of Atmospheric Blocking Using Isentropic Analysis. *Mon. Wea. Rev.,* **116**, 223–241, https://doi.org/10.1175/1520-0493(1988)116<0223:ACSOAB>2.0.CO;2.

7. Dee, D. P., S. M. Uppala, A. J. Simmons, P. Berrisford, P. Poli, S. Kobayashi, U. Andrae, M. A. Balmaseda, G. Balsamo, P. Bauer, P. Bechtold, A. C. M. Beljaars, L. van de Berg, J. Bidlot, 5. N. Bormann, C. Delsol, R. Dragani, M. Fuentes, A. J. Geer, L. Haimberger, S. B. Healy, H. Hersbach, E. V. Hólm, L. Isaksen, P. Kållberg, M. Köhler, M. Matricardi, A. P. McNally, B. M. Monge-Sanz, J.-J. Morcrette, B.-K. Park, C. Peubey, P. de Rosnay, C. Tavolato, J.-N. Thépaut and F. Vitart, 2011: The ERA-Interim reanalysis: configuration and performace of the data assimilation system. *Quart. J. Roy. Meteor. Soc*., **137-656**, Part A, 553–597. doi: 10.1002/qj.828.

8. Eichelberger, S. J., and D. L. Hartmann, 2007: Zonal jet structure and the leading mode of variability. *J. Climate*, **20**, 5149– 5163.

9. Ertel, H., 1942: Ein neuer hydrodynamischer wirbelsatz. Meteor. Z., 59, 271-281.

10. Frederiksen, J.S., 1983: A Unified Three-Dimensional Instability Theory of the Onset of Blocking and Cyclogenesis. II. Teleconnection Patterns. *J. Atmos. Sci.,* **40**, 2593–2609.

11. Griffin, K. S., and J. E. Martin, 2017: Synoptic features associated with temporally coherent modes of variability of the north Pacific jet stream. *J. Climate*, **30**, 39-54.

12. Handlos, Z. J., and J. E. Martin, 2016: Composite analysis of large-scale environments conducive to west Pacific polar/subtropical jet superposition *J. Climate* , **29**, 7145-7165.

13. Henderson, S.A., E.D. Maloney, and E.A. Barnes, 2016: The Influence of the Madden–Julian Oscillation on Northern Hemisphere Winter Blocking. *J. Climate,* **29**, 4597–4616.

14. Hoskins, B.J., I.N. James, and G.H. White, 1983: The Shape, Propagation and Mean-Flow Interaction of Large-Scale Weather Systems. *J. Atmos. Sci.,* **40**, 1595–1612.

15. Hoskins, B.J., and P. D. Sardeshmukh, 1987: A Diagnostic Study of the Dynamics of the Northern-Hemisphere Winter of 1985-1986. *Quart. J. Roy. Meteor. Soc.,* **113**, 759-778.

16. Jaffe, S. C., J. E. Martin, D. J. Vimont, and D. J. Lorenz, 2011: A synoptic-climatology of episodic, sub-seasonal retractions of the Pacific jet. *J. Climate*, **24**, 2846-2860.

17. Jayawardena, I. M and Y. L. Chen, A. J. Nash, K. Kodama, 2012: A Comparison of three prolonged periods of heavy rainfall over the Hawaiian Islands. *J. Appl. Meteor.,* **51**, 722-744.

18. Mak, M., and M. Cai, 1989: Local barotropic instability. J. Atmos. Sci., **46,** 3289–3311.

19. Martius, O., C. Schwierz and H.C. Davies, 2007: Breaking Waves at the Tropopause in the Wintertime Northern Hemisphere: Climatological Analyses of the Orientation and the Theoretical LC1/2 Classification. *J. Atmos. Sci*., **64**, 2576-2592.

20. Nielsen-Gammon, J. W. and R. J. Lefèvre, 1996: Piecewise Tendency Diagnosis of Dynamical Processes Governing the Development of an Upper-Tropospheric Mobile Trough. *J. Atmos. Sci.,* **53**, 3120–3142.

21. Otkin, J. A., and J. E. Martin, 2004. The large-scale modulation of subtropical cyclogenesis in the central and eastern Pacific Ocean. *Mon. Wea. Rev.*, **132**, 1813-1828.

22. Pfahl, S., C. Schweirz, M. Croci-Maspoli, C. M. Grams, & H. Wernli, 2015: Important of latent heat release in ascending air streams for atmospheric blocking. *Nature Geoscience*. **8**, 610-614.

23. Plumb, R.A., 1985: On the Three-Dimensional Propagation of Stationary Waves. *J. Atmos. Sci.,* **42**, 217–229, https://doi.org/10.1175/1520-0469(1985)042<0217:OTTDPO>2.0.CO;2.

24. Rex, D. F., 1950: Blocking action in the middle troposphere and its effect upon regional climate. *Tellus*, **2-3**, 196-211.

25. Trenberth, K.E., 1986: An Assessment of the Impact of Transient Eddies on the Zonal Flow during a Blocking Episode Using Localized Eliassen-Palm Flux Diagnostics. *J.*

Atmos. Sci., **43**, 2070–2087, https://doi.org/10.1175/1520-0469(1986)043<2070:AAOTIO>2.0.CO;2

26. Shutts, G. J., 1983: The propagation of eddies in diffluent jetstreams: Eddy vorticity forcing of ‘‘blocking’’ flow fields. *Quart. J. Roy. Meteor. Soc*., **109**, 737–761.

27. Yamazaki, A. and H. Itoh, 2013: Vortex–Vortex Interactions for the Maintenance of Blocking. Part I: The Selective Absorption Mechanism and a Case Study. *J. Atmos. Sci.,***70**, 725–742.